7 Fusion of Vision Inertial Data for Automatic Georeferencing

D.I.B. Randeniya
Decision Engineering Group
Oak Ridge National Laboratory

M. Gunaratne
Professor
Dept. of Civil and Environment Engineering
University of South Florida
Tampa, FL

S. Sarkar
Professor
Dept. of Computer Science and Engineering
University of South Florida
Tampa, FL

CONTENTS

ABSTRACT

Intermittent loss of the GPS signal is a common problem encountered in intelligent land navigation based on GPS integrated inertial systems. This issue emphasizes the need for an alternative technology that would ensure smooth and reliable inertial navigation during GPS outages. This paper presents the results of an effort where data from vision and inertial sensors are integrated. However, for such integration one has to first obtain the necessary navigation parameters from the available sensors. Due to the variety in the measurements, separate approaches have to be utilized in estimating the navigation parameters. Information from a sequence of images captured by a monocular camera attached to a survey vehicle at a maximum frequency of three frames per second was used in upgrading the inertial system installed in the same vehicle for its inherent error accumulation. Specifically, the rotations and translations estimated from point correspondences tracked through a sequence of images were used in the integration. Also a prefilter is utilized to smoothen out the noise associated with the vision sensor (camera) measurements. Finally, the position locations based on the vision sensor are integrated with the inertial system in a decentralized format using a kalman filter. The vision/inertial integrated position estimates are successfully compared with those from inertial/GPS system output this successful comparison demonstrates that vision can be used successfully to supplement the inertial measurements during potential GPS-outages.

Keywords
Multisensor fusion, inertial vision fusion, intelligent transportation systems.

INTRODUCTION

Inertial navigation systems (INS) utilize accelerometers and gyroscopes in measuring the position and orientation by integrating the accelerometer and gyroscope readings. Long-term error growth, due to this integration, in the measurements of inertial systems is a major issue that limits the accuracy of inertial navigation. However, due to the high accuracy associated with inertial systems in short-term applications, many techniques, such as differential global positioning systems (DGPS), camera (vision) sensors, and others have been experimented by researchers to be used in conjunction with inertial systems and overcome the long-term error growth [1, 2, 3]. But intermittent loss of the GPS signal is a common problem encountered in intelligent land navigation based on GPS integrated inertial systems [3]. This issue emphasizes

the need for an alternative technology that would ensure smooth and reliable inertial navigation *during GPS outages*.

Meanwhile, due to the advances in computer vision, potentially promising studies that involve vision sensing are being carried out in the areas of intelligent transportation systems (ITS) and Automatic Highway Systems (AHS). The above studies are based on the premise that a sequence of digital images obtained from a forward-view camera rigidly installed on a vehicle can be used to estimate the rotations and translations (*pose*) of that vehicle [4]. Hence, a vision system can also be used as a supplementary data source to overcome the issue of time dependent error growth in inertial systems. Therefore, combination of vision technology and inertial technology would be a promising innovation in intelligent transportation systems.

Furthermore, researchers [5] have experimented combining inertial sensors with vision sensors to aid navigation using rotations and translations estimated by the vision algorithm. Roumeliotis et al. [6] designed a vision inertial fusion system for use in landing a space vehicle using aerial photographs and an Inertial Measuring Unit (IMU). The system was designed using an indirect Kalman filter, which incorporates the errors in the estimated position estimation, for the input of defined *pose* from camera and IMU systems. However, the fusion was performed on the relative *pose* estimated from the two sensor systems and due to this reason a much simpler inertial navigation model was used. Testing was performed on a gantry system designed in the laboratory. Chen et al. [7] attempt to investigate the estimation of a structure of a scene and motion of the camera by integrating a camera system and an inertial system. However, the main task of this fusion was to estimate the accurate and robust *pose* of the camera. Foxlin et al. [8] used inertial vision integration strategy in developing a miniature self-tracker, which uses artificial fiducials. Fusion was performed using a bank of Kalman filters designed for acquisition, tracking, and finally perform a hybrid tracking of these fiducials. The IMU data was used in predicting the vicinity of the fiducials in the next image. On the other hand, You et al. [9] developed an integration system that could be used in augmented reality (AR) applications. This system used a vision sensor in estimating the relative position whereas the rotation was estimated using gyroscopes. No accelerometers were used in the fusion. Dial et al. [10] used an IMU and a vision integration system in navigating a robot under indoor conditions. The gyroscopes were used in getting the rotation of the cameras and the main target of the fusion was to interpret the visual measurements. Finally, Huster et al. [4] used the vision inertial fusion to position an autonomous underwater vehicle (AUV) relative to a fixed landmark. Only one landmark was used in this process making it impossible to estimate the pose of the AUV using a camera so that the IMU system is used to fulfill this task.

The approach presented in this paper differs from the above mentioned work in many respects. One of the key differences is that the vision system used in this paper has a much slower frame rate, which introduces additional challenges in autonomous navigation task. In addition, the goal of this work is to investigate a fusion technique that would utilize the *pose* estimation of the vision system in correcting the inherent error growth in IMU system in a GPS deprived environment. Therefore, this system will act as an alternative navigation system until the GPS signal reception is recovered. It is obvious from this objective that this system must incorporate the absolute position in the fusion algorithm rather than the relative position of the two-sensor systems.

FIGURE 7.1 FDOT-Multipurpose survey vehicle.

However, estimating the absolute position from cameras is tedious but the camera data can be easily transformed to the absolute position knowing the initial state. Also in achieving this, one has to carry out more complex IMU navigation algorithm and error modeling. The above developments differentiate the work presented in this chapter from the previous published work. Furthermore, the authors successfully compare a test run performed on an actual roadway setting in validating the presented fusion algorithm.

Multisensor Survey Vehicle

The sensor data for this exercise was collected using a survey vehicle owned by the Florida Department of Transportation (FDOT) (Figure 7.1) that is equipped with a cluster of sensors. Some of the sensors included in this vehicle are

- Navigational grade Inertial Measuring Unit (IMU)
- Two DVC1030C monocular vision sensors
- Two global positioning system (GPS) receivers

The original installation of sensors in this vehicle allows almost no freedom for adjustment of the sensors, which underscores the need for an initial calibration.

Inertial Measuring Unit (IMU)

The navigational grade IMU installed in the vehicle (shown in Figure 7.1) contains three solid state fiber-optic gyroscopes and three solid state silicon accelerometers that measure instantaneous accelerations and rates of rotation in three perpendicular directions. The IMU data is logged at any frequency in the range of 1 Hz–200 Hz.

Due to its high frequency and the high accuracy, at least in short time intervals, in data collection IMU acts as the base for acquiring navigational data. However, due to the accelerometer biases and gyroscope drifts, which are unavoidable, the IMU measurements diverge after a short time. Therefore, in order for the IMU to produce reliable navigational solutions its errors has to be corrected frequently.

Forward-View and Side-View Cameras

The FDOT survey vehicle also uses two high resolution (1300 × 1030) digital area-scan cameras for front-view and side-view imaging at a rate up to 11 frames per second. This enables capturing of digital images up to an operating speed of 60 mph. The front-view camera with a 16.5 mm nominal focal length lens captures the panoramic view, which includes pavement markings, number of lanes, roadway signing, work zones, traffic control and monitoring devices, and other structures.

PREPROCESSING OF RAW DATA

The raw data collected from the different sensors of the vehicle needs to be transformed into useful inputs for the fusion algorithm. In this work two main sensor systems are used, namely the vision system and the IMU. As described in "Multisensor Survey Vehicle" it is understood that these sensor systems need preprocessing to extract the vital navigation parameters such as translations, orientations, velocities, accelerations, and others. Therefore, in this section the most relevant preprocessing techniques in extracting the navigation parameters are illustrated.

Inertial Navigation Fundamentals

The IMU in the vehicle is of strap-down type with three single degree of freedom silicon, or MEMS, accelerometers, and three fiber optic gyroscopes aligned in three mutually perpendicular axes. When the vehicle is in motion the accelerometers measure the specific forces while the gyroscopes measure the rates of change of rotations of the vehicle [11, 12]. Therefore, it is clear that in order to geo-locate the vehicle, one has to integrate the outputs of the accelerometers and gyroscopes with a known initial position.

The angular rates measured by the gyroscopes are rates of change of rotations in the *b-frame,* which has its origin at a predefined location on the sensor and has its first axis toward the forward direction of the vehicle, the third axis toward the direction of gravity, and the second axis toward the right side of the navigation system composing a right-handed coordinate frame, with respect to the *i-frame*, which is a right-handed coordinate frame based on Newtonian mechanics [11, 12], that is, ω_{ib}^{b}. The *n-frame* is defined with the third axis of the system aligned with the local normal to the earth's surface and in the same direction as gravity while the first axis is set along the local tangent to the meridian (north) and the second axis is placed toward the east setting up a right-handed frame. These can be transformed to rotation with respect to the *n-frame* [11] by

$$\omega_{nb}^{b} = \omega_{ib}^{b} - C_{n}^{b}\omega_{in}^{n} \tag{7.1}$$

where, $\omega_{nb}^{b} = (\,\omega_1\ \omega_2\ \omega_3\,)^T$ and ω_{ib}^{b} in Equation (7.1) is the angular rate of the *b-frame* (IMU) with respect to the *i-frame* given in the *b-frame* and n, b represent the *n-frame* and the *b-frame*, respectively. The term C_{n}^{b} denotes the coordinate transformation matrix from the *n-frame* to the *b-frame*. The angular rates of the *n-frame* with respect

to the *i-frame*, ω_{in}^{n}, can be estimated using geodetic coordinates as:

$$\omega_{in}^{n} = [(\dot{\lambda} + \omega_e)\cos(\eta) \; -\dot{\eta} \; -(\dot{\lambda} + \omega_e)\sin(\eta)]^T \tag{7.2}$$

where, $\dot{\lambda}$ and $\dot{\eta}$ denote the rates of change of the longitude and latitude during vehicle travel and ω_e is the earth's rotation rate. Transformation, C_n^b, between the *n-frame* and the *b-frame* can be found, in terms of quaternions, using the following time propagation equation of quaternions:

$$\dot{q} = \frac{1}{2}Aq \tag{7.3}$$

where, q is any unit quaternion that expresses C_n^b and the skew-symmetric matrix $\boldsymbol{A}$ can be given as:

$$\boldsymbol{A} = \begin{pmatrix} 0 & \omega_1 & \omega_2 & \omega_3 \\ -\omega_1 & 0 & \omega_3 & -\omega_2 \\ -\omega_2 & -\omega_3 & 0 & \omega_1 \\ -\omega_3 & \omega_2 & -\omega_1 & 0 \end{pmatrix} \tag{7.4}$$

Finally, using Equations (7.1) to (7.4) one can obtain the transformation (C_n^b) between the *n-frame* and the *b-frame* from the gyroscope measurements in terms of Euler angles. But due to problems inherent in Euler format, such as singularities at poles and the complexity introduced due to trigonometric functions, quaternions are commonly preferred in deriving the differential equation [Equation 7.3].

On the other hand, the accelerometers in the IMU measure the specific force, which can be given as:

$$\ddot{x}^i = g^i(x^i) + a^i \tag{7.5}$$

where, a^i is the specific force measured by the accelerometers in the inertial frame and $g^i(x^i)$ is the acceleration due to the gravitational field, which is a function of the position x^i. From the C_n^b estimated from gyroscope measurement in Equations (7.3) and (7.4) and the specific force measurement from accelerometers in Equation (7.5), one can deduce the navigation equations of the vehicle in any frame. Generally, what is desired in terrestrial navigation are (a) final position, (b) velocity, and (c) orientations be given in the *n-frame* although the measurements are made in another local frame, *b-frame*. This is not possible since the *n-frame* also moves with the vehicle making the vehicle horizontally stationary on this local coordinate frame. Therefore, the desired coordinate frame is the fixed *e-frame,* defined with the third axis parallel to the mean and fixed polar axis, first axis as the axis connecting the center of mass of the earth and the intersection of prime meridian (zero longitude) with the equator, and the second axis making this frame a right-handed coordinate frame. Hence, all the navigation solutions are given in the *e-frame* but along the directions of the *n-frame*. For more detailed description on formulation and explanations please refer [11, 12].

Since both frames considered here (*e-frame* and *n-frame*) are noninertial frames, that is, frames that rotate and accelerate, one must consider the fictitious forces that affect the measurements. Considering the effects of these forces the equation of motion can be written in the navigation frame (*n-frame*) [11, 12] as:

Acceleration

$$\frac{d}{dt}v^n = a^n - \left(\Omega^n_{in} + \Omega^n_{ie}\right)v^n + g^n \tag{7.6}$$

Velocity

$$\frac{d}{dt}x^n = v^n \tag{7.7}$$

The second and third terms in Equation (7.6) are respectively the Coriolis acceleration and the gravitational acceleration of the vehicle. The vector multiplication of the angular rate denoted as Ω has the following form [11]:

$$\Omega = [\omega\times] = \begin{pmatrix}\omega_1\\ \omega_2\\ \omega_3\end{pmatrix}\times = \begin{pmatrix}0 & -\omega_3 & \omega_2\\ \omega_3 & 0 & -\omega_1\\ -\omega_2 & \omega_1 & 0\end{pmatrix} \tag{7.8}$$

On the other hand, the orientation of the vehicle can be obtained [11, 12] by:

$$\frac{d}{dt}C^n_b = C^n_b\Omega^n_{nb} \tag{7.9}$$

In Equation (7.9), Ω^n_{nb} can be obtained using the ω^b_{nb} estimated in Equation (7.1) and then written in the form given in Equation (7.8). Therefore, once the gyroscope and accelerometer measurements are obtained one can setup the complete set of navigation equations by using Equations (7.6) to (7.9). Then one can estimate the traveling velocity and the position of the vehicle by integrating Equations (7.6) and (7.7). The gravitational acceleration can be estimated using the definition of the geoid given in WGS1984 [13]. Then the velocity of the vehicle at any time step $(k+1)$ can be given as:

$$v^n_{(k+1)} = v^n_{(k)} + \Delta v^n \tag{7.10}$$

where, Δv is the increment of the velocity between the kth and $(k+1)$th time interval. The positions can be obtained by integrating Equation (7.10), which then can be converted to the geodetic coordinate frame as:

$$\phi_{(k+1)} = \phi_{(k)} + \frac{(v^n_N)_k\Delta t}{(M_k + h_k)} \tag{7.11}$$

$$\lambda_{(k+1)} = \lambda_{(k)} + \frac{(v^n_E)_k\Delta t}{(N_k + h_k)\cos(\phi_k)} \tag{7.12}$$

$$h_{(k+1)} = h_{(k)} - (v_D)_k\Delta t \tag{7.13}$$

where, v_N, v_E, v_D are, respectively, the velocities estimated in Equation (7.10) in the *n-frame* while, ϕ, λ, and h, are respectively, the latitude, longitude, and height. Moreover, M and N are, respectively, the radii of curvature of the earth at the meridian and the prime vertical passing through the point on earth where the vehicle is located. They are given as follows [11]:

$$N = \frac{p}{\sqrt{(1 - e^2\sin^2\phi)}} \tag{7.14}$$

$$M = \frac{p(1 - e^2)}{(1 - e^2\sin^2\phi)^{3/2}} \tag{7.15}$$

where p is the semimajor axis of the earth and e is the first eccentricity of the ellipsoid.

FIGURE 7.2 Point correspondences tracked in two consecutive images.

ESTIMATION OF *Pose* FROM VISION

When the vehicle is in motion, the forward-view camera can be setup to capture panoramic images at a specific frequency, which will result in a sequence of images. Therefore, the objective of the vision algorithm is to estimate the rotation and translation of the rigidly fixed camera, which are assumed to be the same as those of the vehicle. In this work, *pose* from the vision sensor, that is, forward camera of the vehicle, is obtained by the eight-point algorithm. *Pose* estimation using point correspondences is performed in two essential steps described below.

Extraction of Point Correspondents from a Sequence of Images

In order to perform this task, first it is necessary to establish the feature (point) correspondence between the frames, which will form a method for establishing a relationship between two consecutive image frames. The point features are extracted using the well known KLT (Kanade-Lucas-Tomasi) [14] feature tracker. These point features are tracked in the sequence of images with replacement. Of these feature correspondences only the ones that are tracked in more than five images are identified and used as an input to the eight-point algorithm for estimating the rotation and translation. Thus these features become the key elements in estimating the *pose* from the eight-point algorithm. Figure 7.2 illustrates this feature tracking in two consecutive images.

Estimation of the Rotation and Translation of the Camera Between Two Consecutive Image Frames Using the Eight-Point Algorithm

The algorithm, eight-point algorithm, used to estimate the *pose* requires at least eight noncoplanar point correspondences to estimate the *pose* of the camera between two consecutive images. A description of the eight-point algorithm follows.

Figure 7.3 shows two images captured by the forward-view camera at two consecutive time instances (1 and 2). Point p (in three dimension) is an object captured

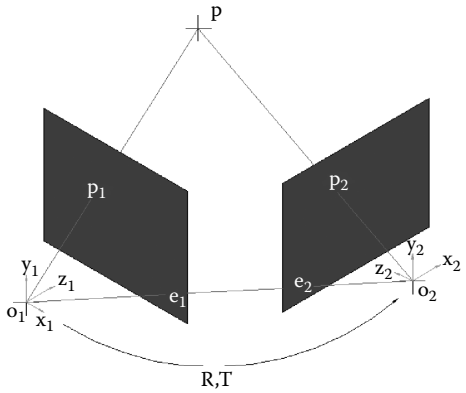

FIGURE 7.3 Schematic diagram for eight-point algorithm.

by both images, and O_1 and O_2 are the camera coordinate frame origins at the above two instances. Points p_1 and p_2 are, respectively, the projections of point p on the two image planes. The *epipoles*, [15] which are points where the lines joining the two coordinate centers and the two image planes intersect, are denoted by e_1 and e_2, respectively. On the other hand, the lines e_1p_1 and e_2p_2 are termed *epipolar lines*. If the rotation and translation between the two images are denoted as $\mathbf{R}$ and T and the coordinates of points p_1 and p_2 are denoted as (x_1, y_1, z_1) and (x_2, y_2, z_2), respectively, then the two coordinate sets can be related as:

$$(x_2 \quad y_2 \quad z_2)^T = \mathbf{R}(x_1 \quad y_1 \quad z_1)^T + \mathrm{T} \tag{7.16}$$

From Figure 7.3 it is clear that the two lines joining p with the camera centers and the line joining the two centers are on the same plane. This constraint, which is geometrically illustrated in Figure 7.3, can be expressed in algebraic form [15] in Equation (7.17). Since the three vectors lie on the same plane:

$$\mathrm{p}_1^T \bullet (\mathrm{T} \times \mathbf{R}\mathrm{p}_2) = 0 \tag{7.17}$$

where, p_1 and p_2 are the homogeneous coordinates of the projection of p onto the two image planes, respectively. Both T, $\mathbf{R}(\in \Re^3)$ are in three-dimensional space, and hence there will be nine unknowns (three elements to represent T in x, y, and z coordinate axes and three elements to represent $\mathbf{R}$ about x, y, and z coordinate axes) involved in Equation (7.17). Since all the measurements obtained from a camera are scaled in depth, one has to solve for only eight unknowns in Equation (7.17). Therefore, in order to find a solution to Equation (7.17) one should meet the criterion;

$$\mathrm{Rank}(\mathrm{T} \times \mathbf{R}) \geq 8 \tag{7.18}$$

Let $\mathbf{E} = \mathrm{T} \times \mathbf{R}$, the unknowns in $\mathbf{E}$ considered as $[e_1\ e_2\ e_3\ e_4\ e_5\ e_6\ e_7\ e_8]$ and the scaled parameter be assumed as 1. Then, one can setup Equation (7.17) as

$$\mathbf{A}\vec{\mathrm{e}} = 0 \tag{7.19}$$

where $\mathbf{A} = (x_1x_2 \quad x_1y_2 \quad x_1f \quad y_1x_2 \quad y_1y_2 \quad y_1f \quad fx_2 \quad fy_2 \quad f^2)$ is a known $n \times 9$ matrix, n being the number of points correspondences established between two images, and, $\vec{e} = [1\ e_1\ e_2\ e_3\ e_4\ e_5\ e_6\ e_7\ e_8]$ is an unknown vector. Once a sufficient number of correspondence points are obtained, Equation (7.18) can be solved and $\vec{e}$ can be estimated. Once the matrix $\mathbf{E}$ is estimated it can be utilized to recover translations and rotations using the relationship $\mathbf{E} = T \times \mathbf{R}$. The translations and rotations can be obtained as,

$$T = c_1 \times c_2$$
$$(T \bullet T)\mathbf{R} = \mathbf{E}^{*T} - T \times \mathbf{E} \tag{7.20}$$

where, $c_i = T \times r_i (\text{for } i = 1, 2, 3)$ and the column vectors of the $\mathbf{R}$ matrix are given as r. Also, $\mathbf{E}^*$is the matrix of cofactors of $\mathbf{E}$. In this chapter, in order to estimate the rotations and translations, a correspondence algorithm that codes the procedure described in Equations (7.16) to (7.20) is used.

Determination of the Transformation Between Vision-Inertial Sensors

Since the vision and the IMU systems are rigidly fixed to the vehicle there exist unique transformations between these two sensor systems. This unique transformation between the two sensor coordinate frames can be determined using a simple optimization technique. In this work it is assumed that the two frames have the same origin but different orientations. First, the orientation of the vehicle at a given position measured with respect to the inertial and vision systems are estimated. Then an initial transformation can be obtained from these measurements. At the subsequent measurement locations, this transformation is optimized by minimizing the total error between the transformed vision data and the measured inertial data. The optimization produces the unique transformation between the two sensors.

In extending the calibration procedures reported in [16] and [17] modifications must be made to the calibration equations in [16] and [17] to incorporate the orientation measurements, that is, roll, pitch, and yaw, instead of three-dimensional position coordinates. The transformations between each pair of the right-handed coordinate frames considered are illustrated in Figure 7.4. In addition, the time-dependent transformations of each system relating the first and second time steps are also illustrated in Figure 7.4. It is shown below how the orientation transformation between the inertial and vision sensors ($\mathbf{R}_{vi}$) can be determined by using measurements, which can easily be obtained at an outdoor setting.

In Figure 7.4 OG, OI, and OV denote origins of global, inertial, and vision coordinate frames, respectively. xk, yk, and zk define the corresponding right-handed three-dimensional–axis system with k representing the respective coordinate frames (i-inertial, v-vision, and g-global). Furthermore, the transformations from the global frame to the inertial frame, global frame to the vision frame, and inertial frame to the vision frame are defined, respectively, as $\mathbf{R}_{ig}$, $\mathbf{R}_{vg}$, and $\mathbf{R}_{vi}$.

If $\mathbf{P}_g$ denotes the position vector measured in the global coordinate frame, the following equations can be written considering the respective transformations between

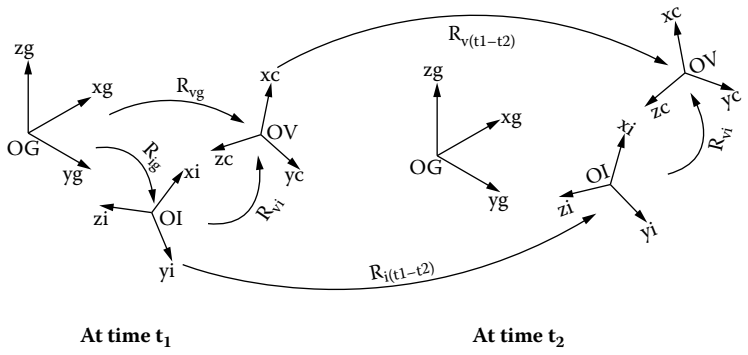

FIGURE 7.4 Three coordinate systems associated with the alignment procedure and the respective transformations.

the global frame and both the inertial and the vision frames.

$$\mathbf{P}_{g(t1)} = \mathbf{R}_{ig(t1)}\mathbf{P}_{i(t1)} \tag{7.21a}$$

$$\mathbf{P}_{g(t1)} = \mathbf{R}_{vg(t1)}\mathbf{P}_{v(t1)} \tag{7.21b}$$

and considering the transformation between the inertial (OI) and vision systems (OV):

$$\mathbf{P}_{i(t1)} = \mathbf{R}_{vi}\mathbf{P}_{v(t1)} \tag{7.22}$$

Substituting Equations (7.21a) and (7.21b) into Equation (7.22), the required transformation can be obtained as;

$$\mathbf{R}_{vi} = \mathbf{R}^{-1}_{ig(t1)}\mathbf{R}_{vg(t1)} \tag{7.23}$$

Although, the transformations between global-inertial and global-vision is time variant, the transformation between the inertial system and the vision system ($\mathbf{R}_{vi}$) is time invariant due to the fact that the vision and inertial systems are rigidly fixed to the vehicle. Once the *pose* estimates for IMU and vision are obtained, the corresponding rotation matrices (in the Euler form) can be formulated considering the rotation sequence of "zyx." Thus, Equation (7.23) provides a simple method of determining the required transformation $\mathbf{R}_{vi}$. Then the Euler angles obtained from this step can be used in the optimization algorithm as initial angle estimates. These estimates can then be optimized as illustrated in the ensuing section to obtain more accurate orientations between x, y, and z axes of the two-sensor coordinate frames.

Optimization of the Vision-Inertial Transformation

If α, β, and γ are the respective orientation differences between the axes of the inertial sensor frame and the vision sensor frame, then the transformation $\mathbf{R}_{vi}$ can be explicitly represented in the Euler form by $\mathbf{R}_{vi}(\alpha, \beta, \gamma)$. Using Equation (7.23) the rotation matrix for the inertial system at anytime t′ can be expressed as

$$\mathbf{R}^{*}_{ig(t')} = \mathbf{R}_{vg(t')}\mathbf{R}^{-1}_{vi}(\alpha, \beta, \gamma) \tag{7.24}$$

$\mathbf{R}_{vg(t')}$ can be determined from a sequence of images obtained using the algorithm described in "Estimation of *pose* from Vision" and $\mathbf{R}^*_{ig(t')}$ can be estimated using Equation (7.24) for any given set (α, β, γ). On the other hand, $\mathbf{R}_{ig(t')}$ also be determined directly from the IMU measurements. Then a nonlinear error function (e) can be formulated in the form:

$$e^2_{pq}(\alpha, \beta, \gamma) = \left[(\mathbf{R}_{ig(t')})_{pq} - (\mathbf{R}^*_{ig(t')})_{pq}\right]^2 \tag{7.25}$$

where p (= 1, 2, 3) and q (= 1, 2, 3) are the row and column indices of the $\mathbf{R}_{ig}$ matrix respectively. Therefore, the sum of errors can be obtained as

$$E = \sum_p \sum_q e^2_{pq}(\alpha, \beta, \gamma) \tag{7.26}$$

Finally, the optimum α, β, and γ can be estimated by minimizing Equation (7.26):

$$\min_{\alpha,\beta,\gamma}\{E\} = \min_{\alpha,\beta,\gamma}\left\{\sum_p \sum_q [(\mathbf{R}_{ig})_{pq} - (\mathbf{R}_{ig(t')})_{pq}]^2\right\} \tag{7.27}$$

Minimization can be achieved by gradient descent [Equation (7.28)] as follows:

$$\mathbf{x}_i = \mathbf{x}_{i-1} - \lambda E'(\mathbf{x}_{i-1}) \tag{7.28}$$

where, $\mathbf{x}_i$ and $\mathbf{x}_{i-1}$ are two consecutive set of orientations, respectively, while λ is the step length and $E'(\mathbf{x}_{i-1})$ is the first derivative of E evaluated at $\mathbf{x}_{i-1}$:

$$E'(\mathbf{x}_{i-1}) = \left[\frac{\partial E(\mathbf{x}_{i-1})}{\partial \alpha} \quad \frac{\partial E(\mathbf{x}_{i-1})}{\partial \beta} \quad \frac{\partial E(\mathbf{x}_{i-1})}{\partial \gamma}\right]^T \tag{7.29}$$

Once the set of angles (α, β, γ) corresponding to the minimum E in Equation (7.27) is obtained, for time step t′, the above procedure can be repeated for a number of time steps t″, t‴, and so on. When it is verified that the set (α, β, γ) is invariant with time it can be used in building the unique transformation $(\mathbf{R}_{vi})$ matrix between the two-sensor systems. A detailed elaboration of this calibration technique could be found in [18].

SENSOR FUSION

IMU Error Model

The IMU navigation solution, described in "Inertial Navigation Fundamentals," was derived from the measurements obtained from gyroscopes and accelerometers, which suffer from measurement, manufacturing, and bias errors. Therefore, in order to develop an accurate navigation solution it is important to model the system error characteristics. In this chapter only the first-order error terms are considered implying that the higher-order terms [13] contribute to only a minor portion of the error. In addition, by selecting only the first-order terms, the error dynamics of the navigation solution

can be made linear with respect the errors [11, 12] enabling the use of Kalman filtering for the fusion.

Error dynamics used in this work were obtained by differentially perturbing the navigation solution [11] by a small increment and then considering only the first order terms of the perturbed navigation solution. Therefore, by perturbing Equations (7.6), (7.7), and (7.9) one can obtain the linear error dynamics for the IMU in the following form [12]:

$$\delta\dot{x} = -\omega_{en}^{n} \times \delta x^{n} + \delta\varphi \times v^{n} + \delta v^{n} \tag{7.30}$$

where δ denotes the small perturbation introduced to the position differential equation [Equation (7.7)] and φ denotes the rotation vector for the position error. And "$\times$" is the vector multiplication of the respective vectors. Similarly, if one perturbs Equation (7.6) the following first-order error dynamic equation can be obtained:

$$\delta v^{n} = C_{b}^{n}\delta a^{b} + C_{b}^{n}a^{b} \times \varepsilon + \delta g^{n} - \left(\omega_{ie}^{n} + \omega_{in}^{n}\right) \times \delta v^{n} - \left(\delta\omega_{ie}^{n} + \delta\omega_{in}^{n}\right) \times v^{n} \tag{7.31}$$

where, ε denotes the rotation vector for the error in the transformation between the *n-frame* and the *b-frame*. The first two terms on the right-hand side of Equation (7.31) are, respectively, due to the errors in specific force measurement and errors in transformation between the two frames, that is, errors in gyroscope measurements. When Equation (7.9) is perturbed one obtains:

$$\delta\dot{\Psi} = -\omega_{in}^{n} \times \varepsilon + \delta\omega_{in}^{n} - C_{b}^{n}\delta\omega_{ib}^{b} \tag{7.32}$$

Equations (7.30) to (7.32) are linear with respect to the error of the navigation equation. Therefore, they can be used in a linear Kalman filter to statistically optimize the error propagation.

Design of the Kalman Filter

In order to minimize the error growth in the IMU measurements, the IMU readings have to be updated by an independent measurement at regular intervals. In this work, vision-based translations and rotations and a master Kalman filter is used to achieve this objective. Since the error dynamics of the IMU is linear, the use of a Kalman filter is justified for fusing the IMU and the vision sensor systems. The architecture for this Kalman filter is illustrated in Figure 7.5.

Design of Vision Only Kalman Filter

The *pose* estimated from the vision sensor system is corrupted due to the various noises present in the *pose* estimation algorithm. Thus it is important to minimize these noises and optimize the estimated *pose* from the vision system. The vision sensor predictions obtained can be optimized using a local Kalman filtering. Kalman filters have been developed to facilitate prediction, filtering and smoothening. In this context it is only used for smoothening the rotations and translations predicted by the vision algorithm. A brief description of this local Kalman filter for the vision system is outlined in this section and a more thorough description can be found in [19].

The states relevant to this work consist of translations, rates of translations, and orientations. Due to the relative ease of formulating differential equations, associated

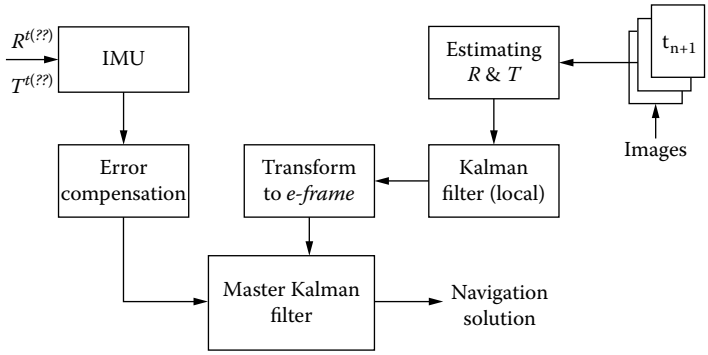

FIGURE 7.5 Schematic diagram of the fusion procedure.

linearity, and the ability to avoid "Gimble-lock," the orientations are expressed in quaternions. Thus, the state vector can be given as

$$X_k = [T_k, \dot{T}_k, q_k]^T \tag{7.33}$$

where, T_k is the translation, q_k is the orientation, given in quaternions, and $\dot{T}_k$ is the rate of translation, at time k. Then the updating differential equations for translations and quaternions can be given as

$$T_{k+1} = T_k + \int_{t_k}^{t_{k+1}} \dot{T}_k dt$$
$$\dot{q}_{k+1} = \left(\frac{1}{2}\right) \mathtt{A} q_k \tag{7.34}$$

where, $\boldsymbol{A}$ is given in Equation (7.4). Then the state transition matrix can be obtained as

$$\phi_k = \begin{pmatrix} \mathbf{I}_{3\times3} & \delta t \mathbf{I}_{3\times3} & \mathbf{0}_{3\times4} \\ \mathbf{0}_{3\times3} & \mathbf{I}_{3\times3} & \mathbf{0}_{3\times4} \\ \mathbf{0}_{4\times3} & \mathbf{0}_{4\times3} & \mathbf{A}_{4\times4} \end{pmatrix} \tag{7.35}$$

where, $\mathbf{I}$ and $\mathbf{0}$ are the identity and null matrices of the shown dimensions, respectively and δt represents the time difference between two consecutive images. The measurements in the Kalman formulation can be considered as the translations and rotations estimated by the vision algorithm. Therefore, the measurement vector can be expressed as

$$Y_k = [T_k, q_k]^T \tag{7.36}$$

Hence, the measurement transition matrix will take the form

$$\mathbf{H}_k = \begin{pmatrix} \mathbf{I}_{3\times3} & \mathbf{0}_{3\times3} & \mathbf{0}_{4\times4} \\ \mathbf{0}_{3\times3} & \mathbf{0}_{3\times3} & \mathbf{I}_{4\times4} \end{pmatrix} \tag{7.37}$$

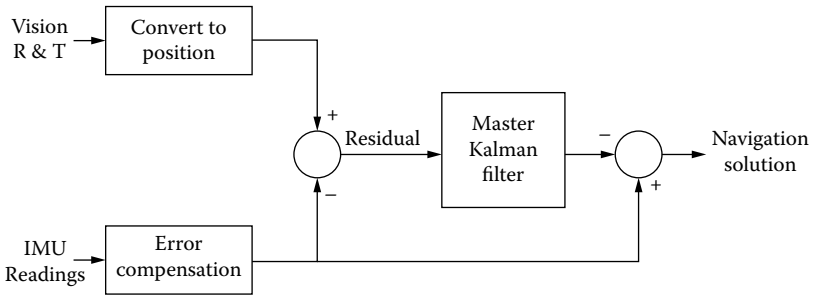

FIGURE 7.6 Illustration of master Kalman filter.

Once the necessary matrices are setup using Equations (7.33) to (7.37), and the initial state vector and the initial covariance matrix are obtained, the vision outputs can be smoothened using the Kalman filter equations. Given Initial conditions can be defined conveniently based on the IMU output at the starting location of the test section.

Design of Master Kalman Filter

The Kalman filter designed to fuse the IMU readings and vision measurements continuously evaluates the error between the two sensor systems and statistically optimizes it. Since the main aim of the integration of the two systems is to correct the high-frequency IMU readings for their error growth, the vision system is used as the updated or precision measurement. Hence, the IMU system is the process of the Kalman filter algorithm. The system architecture of this master Kalman filter is shown in Figure 7.6.

The typical inputs to update the master Kalman filter consists of positions (in the *e-frame*) and the orientations of the *b-frame* and the *c-frame* with respect to the *n-frame*. Since the vision system provides rotations and translations between the camera frames, one needs the position and orientation of the first camera location. These can be conveniently considered as, respectively, the IMU position in the *e-frame*, and the orientation between the *b-frame* and the *n-frame*. The IMU used in the test vehicle is a navigational grade IMU, which has been calibrated and aligned quite accurately. Therefore, the main error that could occur in the IMU measurements is due to biases of gyroscopes and accelerometers. A more detailed explanation of inertial system errors and the design of state equation for the master Kalman fusion algorithm can be found in [20].

Since the IMU error analysis, illustrated in "IMU Error Model," are linear, standard Kalman filter equations can be utilized in the fusion process. There are 16 system states used for the Kalman filter employed in the IMU/vision integration. These are; (a) three states for the position, (b) three states for the velocity, (c) four states for the orientation, which is given in quaternions, and (d) six states for accelerometer and gyroscope biases. Therefore, the state vector for the system (in quaternions) takes the following form:

$$X_k = [\,\delta\phi \;\; \delta\lambda \;\; \delta h \;\; \delta v_n \;\; \delta v_e \;\; \delta v_d \;\; q_w \;\; q_x \;\; q_y \;\; q_z \;\; b_{ax} \;\; b_{ay} \;\; b_{az} \;\; b_{gx} \;\; b_{gy} \;\; b_{gz}\,]^T \tag{7.38}$$

where, δ denotes the estimated error in the state and v_N, v_E, v_D are, respectively, the velocity components along the *n-frame* directions, while ϕ, λ, and h are the latitude, longitude, and height, respectively. The error in the orientation is converted to the quaternion form and its elements are represented as q_i where, $i = w, x, y, z$. And the bias terms in both accelerometers and gyroscopes, that is, $i = a, b$, along three directions, $j = x, y$, and z, are given as b_{ij}. The state transition matrix for this filter would be a 16×16 matrix with the terms obtained from Equations (7.30) to (7.32). The measurements equation is obtained similarly considering the measurement residual.

$$\mathbf{y}_k = [\,(\mathbf{P}_{\mathbf{vis}} - \mathbf{P}_{\mathbf{imu}})\,(\Psi_{\mathbf{vis}} - \Psi_{\mathbf{imu}})\,]^T \tag{7.39}$$

where, $\mathbf{P}_i$ and Ψ_i represent the position vector (3×1) given in geodetic coordinates and the orientation quaternion (4×1), respectively, measured using the ith sensor system with $i =$ vision or IMU. Then the measurement sensitivity matrix would take the form:

$$\mathbf{H}_k = \begin{bmatrix} \mathbf{I}_{3\times3} & \mathbf{0} & \mathbf{0} & \mathbf{0} & \mathbf{0} \\ \mathbf{0} & \mathbf{0} & \mathbf{I}_{4\times4} & \mathbf{0} & \mathbf{0} \end{bmatrix} \tag{7.40}$$

The last critical step in the design of Kalman filter is to evaluate the process (R_k) and measurement (Q_k) variances of the system. These parameters are quite important in the respect that these define the dependability, or the trust, of the Kalman filter on the system and the measurements. The optimum values for these parameters must be estimated on accuracy of the navigation solution or otherwise the noisy input will dominate the filter output making it erroneous. In this work, to estimate R_k and Q_k, the authors used a separate data set; one of the three trial runs on the same section that was not used for the computations performed in this paper. The same Kalman filter was used as a smoother for this purpose. This was important specifically for the vision measurements since it involves more noise in its measurements.

RESULTS

Experimental Setup

The data for the fusion process was collected on a test section on Eastbound State Road 26 in Florida. The total test section was divided into two separate segments; one short run and one relatively longer run. The longer section was selected in such a way that it would include the typical geometric conditions encountered on a roadway, such as straight sections, horizontal curves, and vertical curves. This data was used for the validation purpose of IMU/Vision system with IMU/DGPS system data. The short section was used in estimating the fixed transformation between the two sensor systems.

Transformation Between Inertial and Vision Sensors

Table 7.1 summarizes the optimized transformations obtained for the inertial-vision system. It shows the initial estimates used in the optimization algorithm [Equation (7.24)] and the final optimized estimates obtained from the error minimization

TABLE 7.1
Orientation Difference between Two Sensor Systems Estimated at Short Section

	Initial angle	Optimized angle
	Point 1	
Roll (rad)	−0.00401	−0.03304
Pitch (rad)	−0.00713	0.01108
Yaw (rad)	1.23723	−0.08258
	Point 2	
Roll (rad)	−0.03101	−0.03304
Pitch (rad)	−0.00541	0.01108
Yaw (rad)	1.34034	−0.08258
	Point 3	
Roll (rad)	−0.01502	−0.03304
Pitch (rad)	−0.00259	0.01108
Yaw (rad)	1.32766	−0.08258

process at three separate test locations (corresponding to times t′, t″, and t‴). It is clear from Table 7.1 that the optimization process converges to a unique (α, β, γ) set irrespective of the initial estimates provided. Since the two sensor systems are rigidly fixed to the vehicle, the inertial-vision transformation must be unique. Therefore, the average of the optimized transformations can be considered as the unique transformation that exists between the two sensor systems.

Results of the Vision/IMU Integration

The translations and rotations of the test vehicle were estimated from vision sensors using the point correspondences tracked by the KLT tracker on the both sections. In order to estimate the *pose* from the vision system, the correspondences given in Figure 7.2 were used. Figures 7.7(a)–7.7(c) compare the orientations obtained for both the vision system and the IMU after the vision only Kalman filter.

Similarly, the normalized translations are also compared in Figures 7.8(a)–7.8(c).

It is clear from Figures 7.7 and 7.8 that the orientations and normalized translations obtained by both IMU and filtered vision system match reasonably well. Hence, the authors determined that both sets of data are appropriate for a meaningful fusion and upgrade. These data were then used in the fusion process, described in "Design of Master Kalman Filter," to obtain positions shown in Figures 7.9.

Figure 7.9 compares the vision-inertial fused system with GPS-inertial system and inertial system only. It is obvious from the position estimates, that is, latitude and longitude, that the two systems, vision-inertial and GPS-inertial systems, provide almost the same results with very minute errors. On the other hand, the inertial only measurement deviates as time progresses showing the error growth of the inertial system due to integration of the readings.

TABLE 7.2
Maximum Errors Estimated between IMU/GPS, Vision/IMU, and IMU-Only Measurements

	IMU-GPS	IMU-Vision		IMU-Only		Compared to IMU-Vision Percent Discrepancy of IMU
	Value	Value	Difference	Value	Difference	Only with IMU-GPS
Latitude	0.51741	0.51741	1.496E-07	0.51741	3.902E-07	61.67661
Longitude	−1.44247	−1.44247	4.531E-07	−1.44247	4.183E-07	8.31251

Table 7.2 summarizes the maximum errors shown, in graphical form, in Figure 7.9 between the three sensor units, GPS/IMU, vision/IMU, and IMU-only. For this test run, which lasted only 14 seconds, given in the last column of Table 7.2, the respective latitude and longitude estimates of the IMU/vision system are 61.6% and 8% closer to the IMU/GPS system than the corresponding estimates of IMU-only system. The error

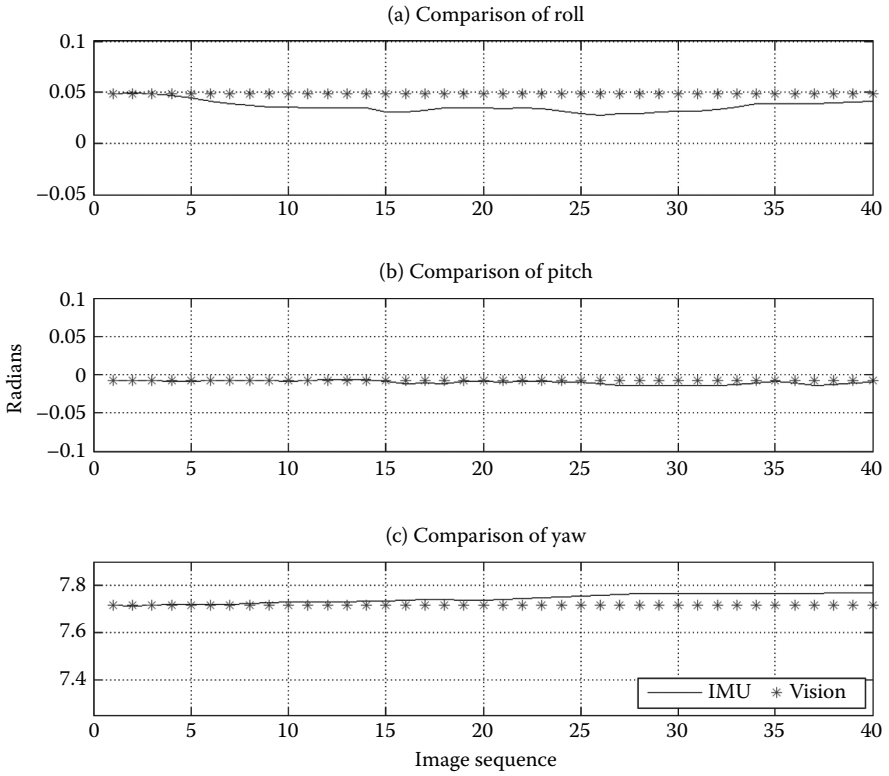

FIGURE 7.7 Comparison of (a) Roll, (b) Pitch, and (c) Yaw of IMU and filtered vision.

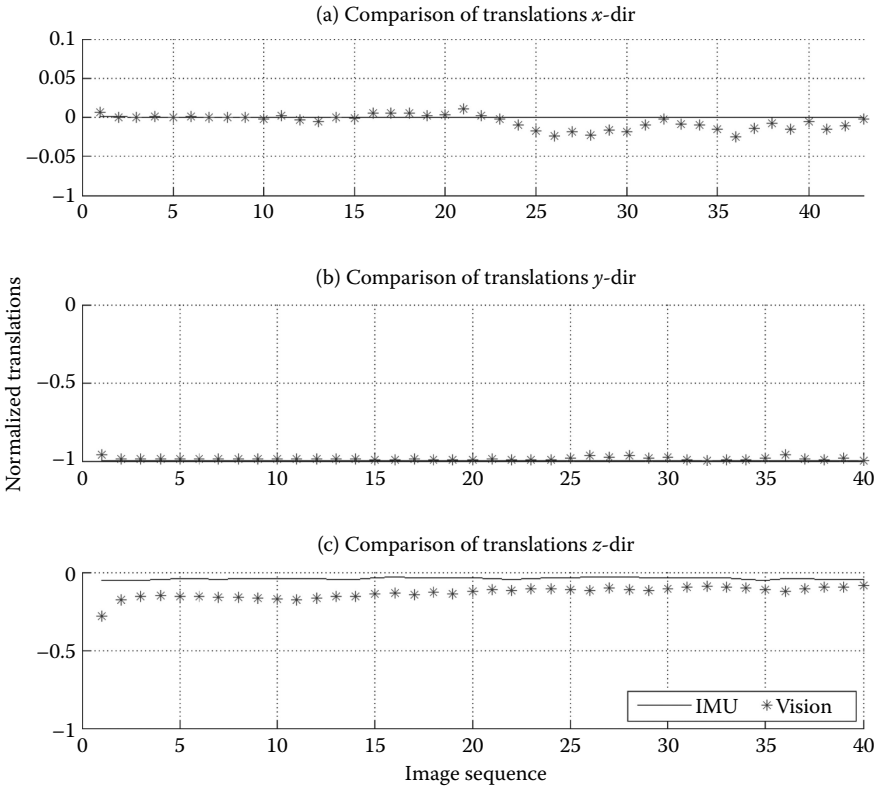

FIGURE 7.8 Comparison of translations (a) x-direction, (b) y-direction, and (c) z-direction.

estimated from the Kalman filter is given in Figure 7.10. It is clear from Figure 7.10 that the error in the fusion algorithm minimizes as the time progresses indicating that the fusion algorithm has acceptable performances.

Figure 7.9 shows that the position, i.e. latitude and longitude, estimated by the vision/IMU integration agree quite well with that given by the IMU/DGPS integration. Thus, these results clearly show that the vision system can supplement the IMU measurements during a GPS outage. Furthermore, the authors have investigated the error estimation of the vision/IMU fusion algorithm in Figure 7.10. Figure 7.10 shows that the Kalman filter used for fusion achieves convergence and also that the error involved in the position estimation reduces with time. These results are encouraging since it further signifies the potential use of the vision system as an alternative to GPS in updating IMU errors.

CONCLUSION

This work addresses two essential issues that one would come across in the process of fusing vision and inertial sensors: (a) estimating the necessary navigation parameters,

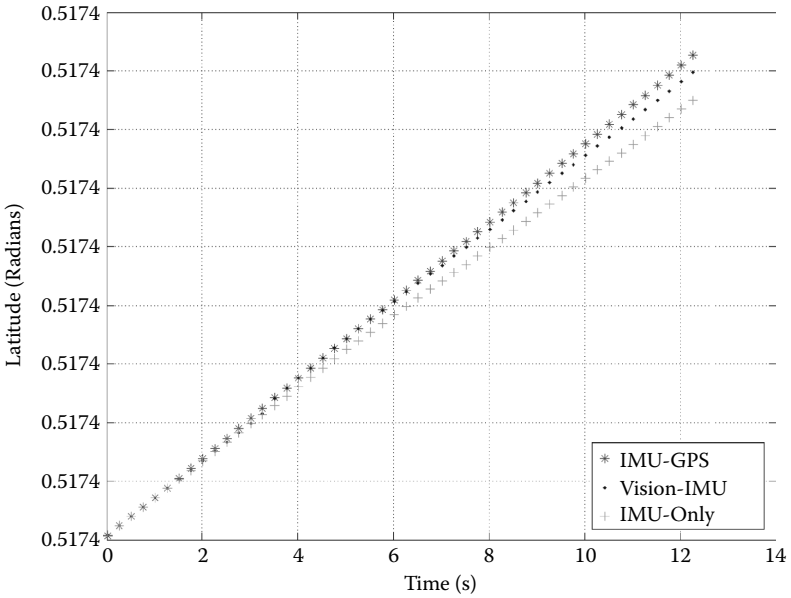

(a) Latitude

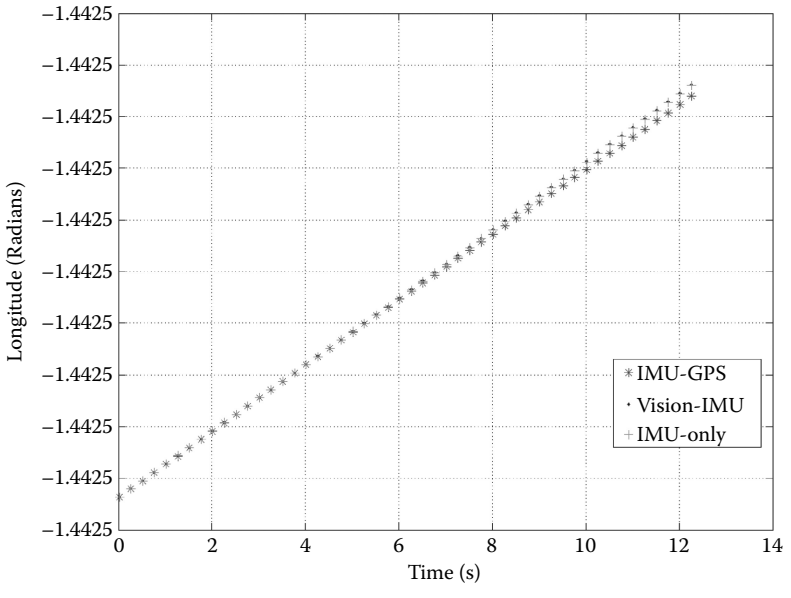

(b) Longitude

FIGURE 7.9 Comparison of (a) latitude and (b) longitude.

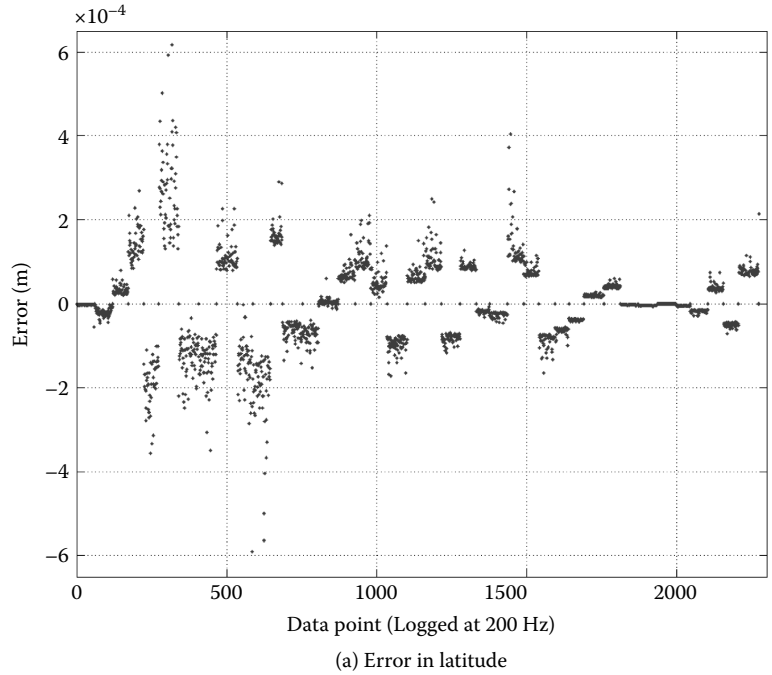

(a) Error in latitude

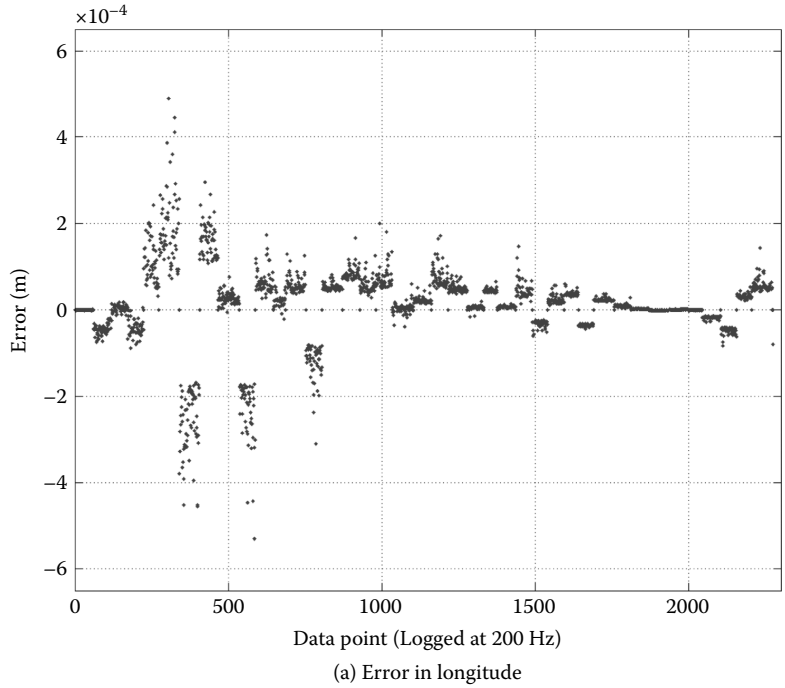

(a) Error in longitude

FIGURE 7.10 Error associated with (a) latitude and (b) longitude.

and (b) fusing the inertial sensor and the vision sensor in an outdoor setting. The fixed transformation between the two sensor systems was successfully estimated, Table 7.1, and validated by comparing with the IMU measurements. The results also showed that the vision data can be used successfully in updating the IMU measurements against the inherent error growth. The fusion of vision/IMU measurements was performed for a sequence of images obtained on an actual roadway and compared successfully with the IMU/DGPS readings. The IMU/DGPS readings were used as the basis for comparison since the main task of this work was to explore an alternative reliable system that can be used successfully in situations where the GPS signal is unavailable.

BIOGRAPHIES

Duminda I.B. Randeniya Duminda Randeniya obtained his BSc (Eng) in Mechanical Engineering with honors at University of Peradeniya Sri Lanka, in 2001. He pursued postgraduate education with a MS in Applied Mathematics, concentration on Control Theory, from Texas Tech University at Lubbock, TX in 2003 and a PhD in Intelligent Transportation Systems, concentration on multi-sensor fusion, from University of South Florida at Tampa, FL in 2007.

He worked as a temporary lecturer at Department of Mechanical Engineering, University of Peradeniya, Sri Lanka from 2001-2002. He currently works as a Post-Doctoral Research Associate in Decision Engineering Group. His research interests are intelligent transportation systems, data mining and statistical forecasting.

Manjriker Gunaratne Manjriker Gunaratne is Professor of Civil Engineering at the University of South Florida. He obtained his Bachelor of Science in Engineering (Honors) degree from the Faculty of Engineering, University of Peradeniya, Sri Lanka. Subsequently, he pursued post-graduate education earning Master of Applied Science and the doctoral degrees in Civil Engineering from the University of British Columbia, Vancouver, Canada and Purdue University, USA respectively. During 22 years of service as an engineering educator, he has authored 30 papers that were published in a number of peer-reviewed journals such as the American Society of Civil Engineering (Geotechnical, Transportation, Civil Engineering Materials and Infrastructure systems) journals, International Journal of Numerical and Analytical Methods in Geomechanics, Civil Engineering Systems and others. In addition he has made a number of presentations at various national and international forums in geotechnical and highway engineering.

He has been involved in a number of research projects with the Florida Department of Transportation, U.S. Department of the Air Force and the National Aeronautics and Space Administration (NASA). He has also held Fellowships at the U.S. Air Force (Wright-Patterson Air Force Base) and NASA (Robert Goddard Space Flight Center) and a Consultant's position with the United Nations Development Program (UNDP) in Sri Lanka. In 1995, at the University of South Florida, he was awarded the Teaching Incentive Program (TIP) award. He has also served as a panelist for the National Science Foundation (NSF) and a member of the Task force for investigation of dam failures in Florida, USA.

Sudeep Sarkar Sudeep Sarkar received the B Tech degree in Electrical Engineering from the Indian Institute of Technology, Kanpur, in 1988. He received the MS and PhD degrees in Electrical Engineering, on a University Presidential Fellowship, from The Ohio State University, Columbus, in 1990 and 1993, respectively. Since 1993, he has been with the Computer Science and Engineering Department at the University of South Florida, Tampa, where he is currently a Professor. His research interests include perceptual organization in single images and multiple image sequences, automated American Sign Language recognition, biometrics, gait recognition, and performance evaluation of vision systems. He is the coauthor of the book "Computing Perceptual Organization in Computer Vision," published by World Scientific. He also the coeditor of the book "Perceptual Organization for Artificial Vision Systems" published by Kluwer Publishers.

He is the recipient of the National Science Foundation CAREER awardin 1994, the USF Teaching Incentive Program Award for undergraduate teaching excellence in 1997, the Outstanding Undergraduate Teaching Award in 1998, and the Theodore and Venette Askounes-Ashford Distinguished Scholar Award in 2004. He served on the editorial boards for the IEEE Transactions on Pattern Analysis and Machine Intelligence (1999-2003) and Pattern Analysis & Applications Journal during (2000-2001). He is currently serving on the editorial board of the Pattern Recognition journal and the IEEE Transactions on Systems, Man, and Cybernetics, Part-B.

REFERENCES

1. Cramer M., GPS/INS Integration. [Online]. http://www.ifp.unistuttgart.de/publications/phowo97/cramer.pdf December, 2005.
2. Wei M., Schwarz K. P., "Testing a decentralized filter for GPS/INS integration," *Position Location and Navigation Symposium, IEEE Plans*, March 1990.
3. Feng S., and Law C. L., "Assisted GPS and its Impact on Navigation Transportation Systems," *Proceedings of the 5th IEEE International Conference on ITS*, Singapore, September 3–6, 2002.
4. Huster A., and Rock S., "Relative Position Sensing by Fusing Monocular Vision and Inertial Rate Sensors," *Proceeding of the 11th International Conference on Advanced Robotics*, Portugal, 2003.
5. Sotelo M., Rodriguez F., and Magdalena L., "VIRTUOUS: Vision-Based Road Transportation for Unmanned Operation on Urban-Like Scenarios," *IEEE Trans*. On ITS, Vol. 5, No. 2, June 2004.
6. Roumeliotis S.I., Johnson A.E., and Montgomery J.F., "Augmenting inertial navigation with image-based motion estimation," *Proceedings of the 2002 IEEE on International Conference on Robotics & Automation*, Washington DC, 2002.
7. Chen J., and Pinz A., "Structure and Motion by Fusion of Inertial and Vision-Based Tracking," *Proceedings of the 28th OAGM/AAPR Conference*, Vol. 179 of Schriftenreihe, 2004, pp. 55–62.
8. Foxlin E., and Naimark L., "VIS-Tracker: A Wearable Vision-Inertial Self-Tracker," IEEE VR2003, Los Angeles CA, 2003.
9. You S., and Neumann U., "Fusion of Vision and Gyro Tracking for Robust Augmented Reality Registration," *IEEE conference on Virtual Reality 2001*, 2001.

10. Dial D., DeBitetto P., and Teller S., "Epipolar Constraints for Vision-Aided Inertial Navigation," *Proceedings of the IEEE Workshop on Motion and Video Computing (WACV/MOTION 05)*, 2005.
11. Jekeli C., "Inertial Navigation Systems with Geodetic Applications," Walter de Gruyter GmbH & Co., Berlin, Germany, 2000.
12. Titterton D.H., and Weston J.L., "Strapdown inertial navigation technology," in *IEE Radar, Sonar, Navigation and Avionics* Series 5, E. D. R. Shearman and P. Bradsell, Ed. London: Peter Peregrinus Ltd, 1997, pp. 24–56.
13. Shin EH, "Estimation of Techniques for Low Cost Inertial Navigation," PhD dissertation, University of Calgary, CA, 2005.
14. Birchfield S. (2006 November), "KLT: An Implementation of the Kanade-Lucas-Tomasi Feature Tracker" [online]. http://www.ces.clemson.edu/∼stb/klt/
15. Faugeras O., *Three Dimensional Computer Vision: A Geometric Viewpoint*, 2nd edition, MIT press, Cambridge, Ma, 1996.
16. Alves J., Lobo J., and Dias J., "Camera-Inertial Sensor Modeling and Alignment for Visual Navigation," *Proceedings of 11th International Conference on Advanced Robotics*, Coimbra, Portugal, June 2003.
17. Lang P., and Pinz A., "Calibration of Hybrid Vision/Inertial Tracking Systems," *Proceedings of 2nd Integration of Vision and Inertial Sensors*, Barcelona, Spain, April 2005.
18. Randeniya D., Gunaratne M., Sarkar S., and Nazef A., "Calibration of Inertial and Vision Systems as a Prelude to Multi-Sensor Fusion," Accepted for publication by Transportation Research Part C (Emerging Technologies), Elsevier, June 2006.
19. Randeniya D., Sarkar S. and Gunaratne M., "Vision IMU Integration using Slow Frame Rate Monocular Vision System in an Actual Roadway Setting," Under review by the *IEEE Intelligent Transportation Systems*, May 2007.